Outphasing Energy Recovery Amplifier With Resistance Compression for Improved Efficiency

Philip A. Godoy, *Student Member, IEEE*, David J. Perreault, *Senior Member, IEEE*, and Joel L. Dawson, *Member, IEEE*

***Abstract*—We describe a new outphasing energy recovery amplifier (OPERA) which replaces the isolation resistor in the conventional matched combiner with a resistance-compressed rectifier for improved efficiency. The rectifier recovers the power normally wasted in the isolation resistor back to the power supply, while a resistance compression network (RCN) reduces the impedance variation of the rectifier as the output power varies. Because the combiner requires a fixed resistance at the isolation port to ensure matching and isolation between the two outphased power amplifiers (PAs), the RCN serves to maintain high linearity as well as high efficiency in the switching-mode PAs. For demonstration, a prototype OPERA system is designed and implemented with discrete components at an operating frequency of 48 MHz, delivering 20.8 W peak power with 82.9% PAE. The measurement results show an efficiency improvement from 17.9% to 42.0% for a 50-kHz 16-QAM signal with a peak-to-average power ratio of 6.5 dB.**

***Index Terms*—Linear amplification with nonlinear components (LINC), outphasing, radio-frequency (RF) power amplifier, resistance compression.**

I. Introduction

THE outphasing power amplifier concept dates back to the early 1930s as an approach for the simultaneous realization of high-efficiency and high-linearity amplification [1]. The principle of outphasing, also known as linear amplification of nonlinear components (LINC) [2], is shown in Fig. 1. The fundamental idea of the LINC architecture is to decompose the signal to be amplified into two constant-envelope signals that are phase-modulated such that their vector sum reproduces the orginal signal. Since the two signals are constant-envelope, they can be amplified by highly efficient—and highly nonlinear—power amplifiers (PAs), including partially and fully switched-mode designs such as class E [3], [4], class F [5]–[7], class E/F [8], class F^{-1} [9], class Φ [10], class Φ_2 [11], etc. The output of the two PAs are then summed with a power combiner at the output to produce an amplified version of the input. The key advantage of this approach is that each amplifier can operate in an efficient albeit nonlinear mode, and yet the final output can be highly linear, breaking the usual tradeoff between linearity and efficiency in power amplifiers.

Manuscript received June 16, 2009; revised September 22, 2009. First published November 13, 2009; current version published December 09, 2009. This work was funded in part by the MIT Deshpande Center and by the MIT Center for Integrated Circuits and Systems.

P. A. Godoy, D. J. Perreault, and J. L. Dawson are with the Department of Electrical Engineering and Computer Science, Massachusetts Institute of Technology, Cambridge, MA 02139 USA (e-mail: godoy@mit.edu; djperrea@mit.edu; jldawson@mtl.mit.edu).

Color versions of one or more of the figures in this paper are available online at http://ieeexplore.org.

Digital Object Identifier 10.1109/TMTT.2009.2033976

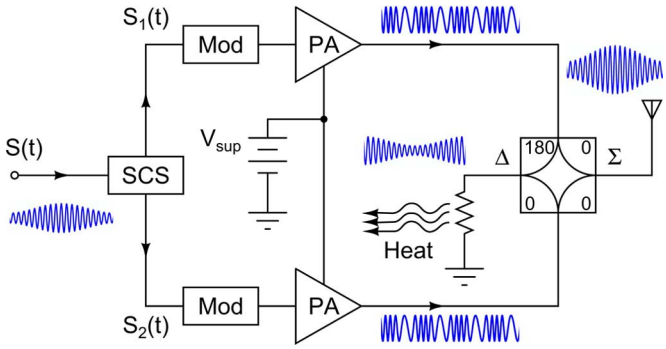

Fig. 1. Outphased power amplifier illustrating power wasted in combining network.

However, one of the major disadvantages of the LINC architecture is the power wasted in the power combiner. To avoid signal distortion and preserve switching amplifier efficiency, an isolating combiner such as a Wilkinson combiner must be used, which isolates the two outphased PAs and provides a fixed impedance load to each PA. Isolating combiners achieve 100% efficiency only at maximum output power. When the inputs are outphased to vary the amplitude, power is wasted as heat in the isolation resistor [12], as shown in Fig. 1. Since the power delivered to the combiner by the two PAs is constant, the efficiency of the LINC system is directly proportional to the output power sent to the antenna load. The time-averaged efficiency is therefore inversely proportional to the peak-to-average power ratio (PAPR). Unfortunately, high-level modulation schemes such as 64-QAM and OFDM tend to have high PAPR, leading to low average efficiency when the LINC system is used.

To alleviate the problem of wasted energy during outphasing, nonisolating combiners are sometimes used. The Chireix combiner is a prominent example, which uses compensating reactive elements to enhance the power-combining efficiency [1], [12], [13]. However, the Chireix combiner can only be tuned for a very small range of outphase angles. With outphase angles outside the tuned range, the load impedance presented to the PAs deviates too far from the nominal value and the isolation between the two power amplifiers' outputs becomes poor. The result is significant distortion and degraded PA efficiency. Adaptive termination of each amplifier output depending on the outphase angle was applied in [14] to improve the combiner efficiency over a much larger range of outphase angles, but at the expense of great circuit complexity.

A power recycling technique was proposed in [15] and [16] as an attempt to enhance the power efficiency of the LINC architecture without giving up the simplicity of an isolating combiner. The principle of the power reuse technique is shown in Fig. 2, in

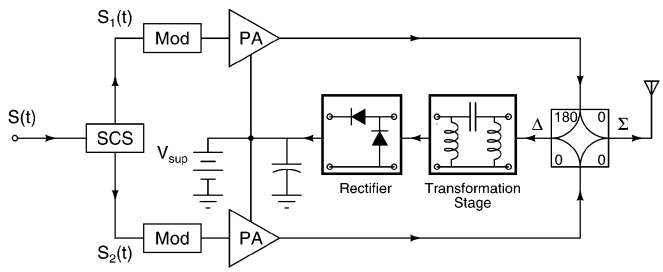

Fig. 2. Outphasing power amplifier with power recycling network.

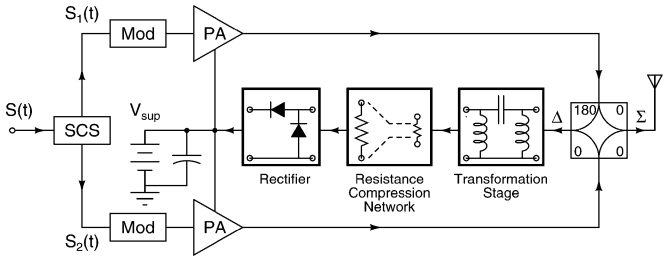

Fig. 3. Proposed outphasing energy recovery amplifier, utilizing a resistance compression network in the power recycling network.

which the isolation resistor is replaced with an RF-dc converter to recover the wasted power back to the power supply. While this approach has been shown to result in a significant increase in the overall efficiency, the implementation in [15] and [16] still suffers from excessive impedance variation at the isolation port and therefore incomplete isolation between the two PAs. This can lead to excessive signal distortion and lower efficiency or even breakdown in the PAs, particularly those sensitive to load impedance (e.g., class-E amplifiers). An additional isolator can be added between the isolation port and the RF-dc converter to reduce this effect, but at the cost of added complexity and loss.

We propose a new outphasing energy recovery amplifier (OPERA) architecture, shown in Fig. 3, which substantially reduces the impedance variation at the isolation port of the combiner through the use of a resistance compression network (RCN) [17]. The RCN improves the matching and isolation between the two outphased PAs, helping to maintain high linearity as well as high efficiency in the switching-mode PAs.

The outline of this paper is as follows. In Section II, we describe the OPERA system, including the resistance-compressed rectifier which recovers the untransmitted power from the PAs. Section III describes the experimental prototype, and in Section IV, we present our measured results. Finally, conclusions are drawn in Section V.

II. OPERA System

The OPERA system shown in Fig. 3 recovers the power normally wasted in the isolation resistor back to the power supply by replacing the resistor with a RF-dc converter. However, a rectifier alone is not enough because the equivalent input impedance of the rectifier varies with input power, as explained in detail below. This impedance variation reduces the isolation between the two PAs, lowering the PA efficiency (and even possibly causing complete malfunction) and increasing signal distortion at the output. We use an RCN to reduce the rectifier impedance variation thereby mitigating this effect.

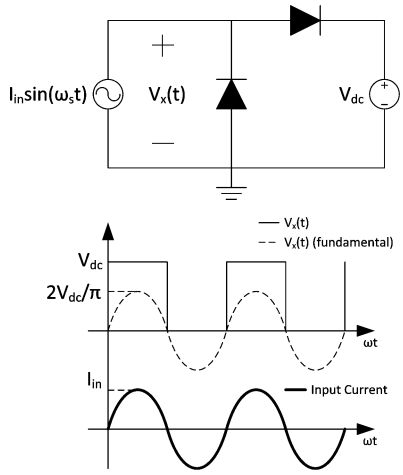

Fig. 4. Ideal half-wave rectifier with constant voltage load and driven by a sinusoidal current source, along with characteristic waveforms. The input current and the fundamental of the input voltage are in phase.

As the final step, an impedance transformation stage is placed between the RCN and the combiner's isolation port to match the resistance-compressed rectifier impedance to the impedance required by the power combiner.

A. Resistance-Compressed Rectifier

Because the combiner requires a fixed resistance at the isolation port to ensure matching and isolation between the two outphased PAs, the RF-dc converter which recovers the wasted power should provide a constant resistive impedance at its input. A purely resistive input impedance can be achieved with a variety of rectifier structures. One example of this kind of rectifier is an ideal half bridge rectifier driven by a sinusoidal current source of amplitude $I_{\rm in}$ and frequency ω_s, and having a constant output voltage $V_{\rm dc}$, as shown in Fig. 4. The voltage at the input terminals of the rectifier $v_x(t)$ will be a square wave having a fundamental component of amplitude $V_{x1} = (2V_{\rm dc}/\pi)$ in phase with the input current $i_{\rm in}(t)$. The electrical behavior at the fundamental frequency ω_s (neglecting harmonics) can be modelled as a resistor of value $R_{\rm eq} = (2/\pi)(V_{\rm dc}/I_{\rm in})$. There are many other types of rectifier topologies that present the above-mentioned behavior (see, e.g., [18]); another is the resonant rectifier of [17] and [19]. Driving such a rectifier with a tuned network suppresses the harmonic content inherent in its operation and results in a resistive impedance characteristic at the desired frequency. This equivalent resistance can be represented by

$$R_{\rm rect} = k_{\rm rect}\frac{V_{\rm dc}}{|I_1|} \tag{1}$$

where $k_{\rm rect}$ depends on the specific rectifier structure and $|I_1|$ is the fundamental component of the drive current. Ignoring harmonics, the power delivered to the rectifier is $P_{\rm in} = (1/2)I_{\rm in}^2 R_{\rm rect}$, and we can write the rectifier impedance as

$$R_{\rm rect} = \frac{(k_{\rm rect}V_{\rm dc})^2}{2P_{\rm in}}. \tag{2}$$

Equation (2) shows that the rectifier input impedance is inversely proportional to input power. Since the power delivered to the isolation port of the combiner in the LINC system varies

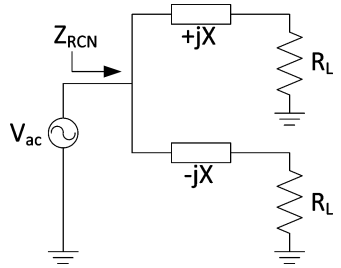

Fig. 5. Two-element resistance compression network with reactive branches represented by impedances evaluated at the operating frequency.

with the outphasing angle between the two PAs, the impedance of a rectifier placed at the isolation port will vary as well. The result is incomplete isolation between the outphased PAs, leading to distortion and lower PA efficiency.

In order to improve the isolation, we introduce an RCN before the rectifier as shown in Fig. 3 to reduce the impedance variation of the rectifer. As described in [17], an RCN can be combined with an appropriate set of rectifiers to yield an RF-dc converter with narrow-range resistive input characteristics. Fig. 5 shows how a pair of rectifiers can be used with an RCN to build a rectifier system having a resistive input characteristic that varies little as the input power changes. The RCN applied here consists of two conjugate reactances, each in series with one of two matched load resistances representing the equivalent resistances of two rectifiers as given by (2). The reactive branches are designed to have the specified reactance X at the desired operating frequency. It can be shown that at this frequency the input impedance of the network will be resistive with a value

$$R_{\mathrm{RCN}} = \frac{X^2}{2R_{\mathrm{rect}}}\left[1+\left(\frac{R_{\mathrm{rect}}}{X}\right)^2\right] \tag{3}$$

which provides compression of the matched load resistances R_{rect} about a center value of impedance X. For variations of R_{rect} over a range having a geometric mean of X (i.e., $R_{\mathrm{rect}} \in [(X/\sqrt{c_{\mathrm{rect}}}), \sqrt{c_{\mathrm{rect}}}X]$, where c_{rect} is the ratio of the largest to smallest resistances in the R_{rect} range), the corresponding ratio of the compressed R_{RCN} range can be shown to be

$$c_{\mathrm{RCN}} = \frac{1+c_{\mathrm{rect}}}{2\sqrt{c_{\mathrm{rect}}}}. \tag{4}$$

For example, a $10:1$ variation in $R_{\mathrm{rect}}(c_{\mathrm{rect}} = 10)$ results in a modest $1.74:1$ variation in R_{RCN}. Since R_{rect} is inversely proportional to P_{in} as shown in (2), this means a $10:1$ variation in power delivered to the isolation port would result in only a $1.74:1$ variation in isolation port resistance. This narrowed range of resistance will result in substantially improved isolation between the two outphased PAs, greatly improving their efficiency.

It should be noted that at sufficiently low outphasing angles (corresponding to small amounts of power delivered to the rectifiers), the rectifier resistance can no longer be effectively compressed. The reason is that at low input power levels, the diodes will be unable to turn "on" and overcome the combination of supply voltage and diode built-in potential. When the diodes turn "off," (1) and (2) no longer hold, and furthermore, the efficiency of the power recycling network drops considerably. However, this poses no serious problems. In this region of operation, most of the power from the PAs is delivered to the antenna load, and so the isolation port acts as a virtual open circuit. Therefore, the rectifier impedance and the efficiency of the recycling network do not matter.

B. RCN Bandwidth

Equation (3) shows how the RCN in Fig. 5 reduces the impedance variation of two matched load resistances. However, this equation is only valid at a single operating frequency, when the two reactances in the RCN are equal in magnitude and opposite in sign. For many applications (e.g., wireless communications), wideband operation centered around a specified RF frequency is desired. Thus, it is important to consider the bandwidth limitations of the RCN.

Let us consider the case in which the reactances of the RCN in Fig. 5 are implemented with a single inductor and capacitor. In this case, we can write the impedance of the RCN as

$$Z_{\mathrm{RCN}} = \left(R+\frac{1}{j\omega C}\right) \| (R+j\omega L) \tag{5}$$

$$= \left(R - jZ_o\frac{1}{\frac{\omega}{\omega_o}}\right) \| \left(R + jZ_o\frac{\omega}{\omega_o}\right) \tag{6}$$

where C is the capacitance, L is the inductance, $Z_o = \sqrt{L/C}$ is the characteristic impedance of the tank [equal to the reactance X in (3)], and ω/ω_o is the ratio of the driving frequency to the center frequency. It can be seen that (6) reduces to (3) when $\omega = \omega_o$. When the frequency deviates from the center frequency, one of the two branches in the RCN will dominate over the other, such that the RCN impedance is no longer purely resistive but also either capacitive or inductive, depending on the direction of the frequency deviation and the value of the load resistance. When such an impedance is presented to a PA, the result is degraded linearity and efficiency.

Fig. 6 shows the RCN impedance versus load resistance for a frequency deviation of $\pm 5\%$ of the center operating frequency. This represents a bandwidth of 10% of the center frequency, which is wide enough for most applications. Over this frequency range, the figure shows that the RCN still effectively compresses the load resistance over a large range, with only a modest reactive component in the total impedance. For a $10:1$ load resistance variation, the maximum deviation in impedance phase is only $\pm 7.5^\circ$ with virtually no deviation in impedance magnitude. This amount of impedance variation should be suitable for most applications.

It should be noted that multiple RCNs can be cascaded to achieve even higher levels of resistance compression to further increase the bandwidth of the RCN for a given RCN impedance variation and load resistance variation [17]. For example, the impedances Z_{RCN} in Fig. 5 can each represent the load impedance of subsequent RCN stages. An "N-stage" compression network would thus have 2^N load resistances that vary in a matched fashion. However, the efficacy of many-stage compresssion is likely to be limited by a variety of practical considerations.

The analysis presented here assumed ideal load resistances with no reactive component. The situation is more complicated when the load resistances are rectifiers, since the rectifier impedance is not always purely resistive in practical implementations, where the parasitic diode capacitance must be taken

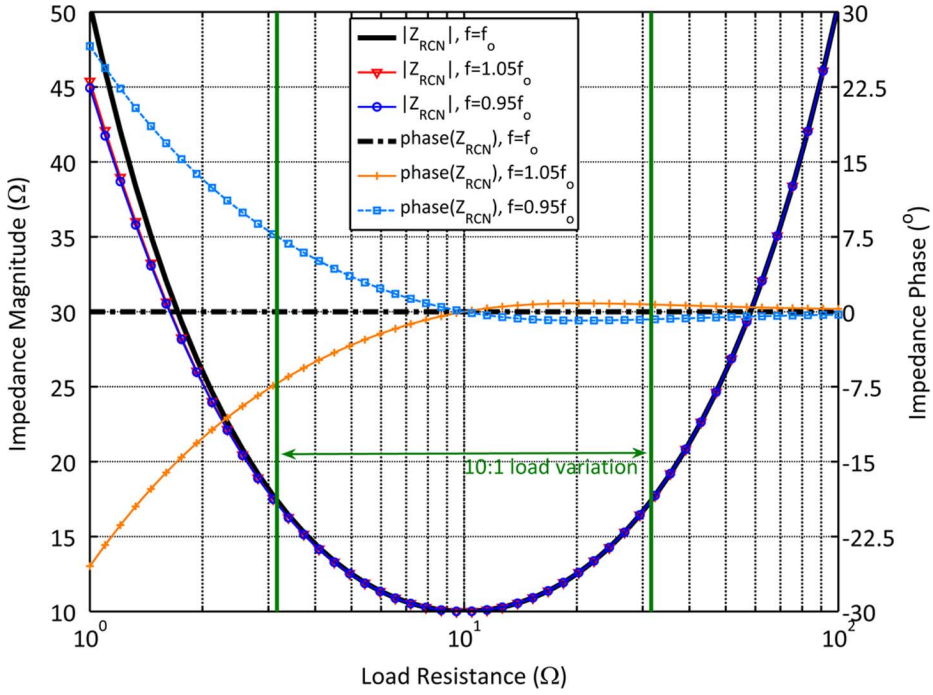

Fig. 6. RCN impedance versus load resistance for a frequency deviation of $\pm 5\%$ of the center operating frequency. $Z_o = X = 10\ \Omega$.

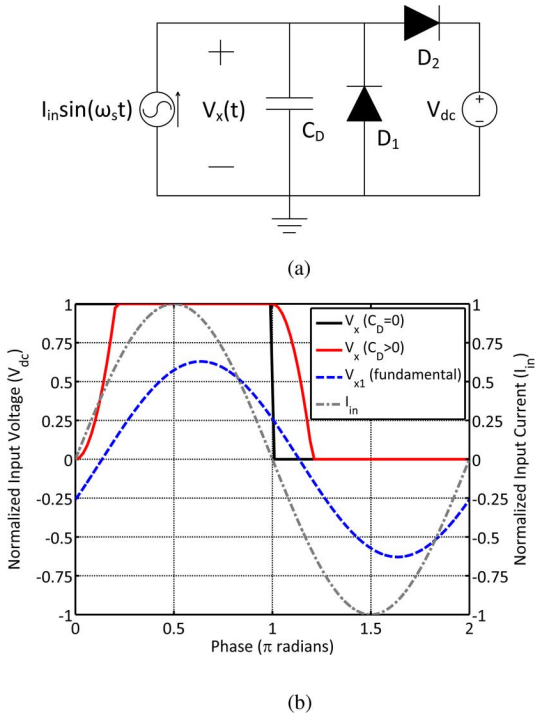

Fig. 7. Half-wave rectifier with parasitic capacitance and driven by a sinusoidal current source, along with characteristic waveforms. (a) Half-wave rectifier with parasitic capacitance. (b) Time-domain input voltage and current.

into account. The effect of parasitic capacitance on the rectifier impedance will be considered in next section.

C. Rectifier Impedance With Parasitic Capacitance

In Section II-A, it was shown that the ideal half-wave rectifier has a purely resistive input impedance given by (1). However, this is not true if the parasitic diode junction capacitance is taken into account [20]. Fig. 7(a) shows the half-wave rectifier with parasitic capacitance C_D, representing the total equivalent capacitance of the two diodes. The capacitance C_D prevents the input voltage V_x from changing abruptly, resulting in the waveforms shown in Fig. 7(b). The figure shows that the fundamental component of the input voltage is no longer in phase with the input current, resulting in a rectifier impedance that is no longer purely resistive but also partially capacitive, as one might expect. This is undesirable because the PA efficiency and linearity degrade when the load impedance is not purely resistive. The RCN can compensate for this by providing a certain amount of "phase compression" [17], but only to a limited extent. The rectifier impedance in the presence of parasitic capacitance can be determined by calculating the Fourier series coefficients of the input voltage waveform V_x.

Referring to Fig. 7(b), there are four distinct time intervals of the V_x waveform that we must describe in order to do the Fourier analysis. During the first time interval, both diodes are off and the capacitance C_D is being charged by the input current source. During this time, the input voltage V_x is given by

$$V_x(t) = \frac{I_{\rm in}}{\omega_s C_D}[1 - \cos(\omega_s t)] \tag{7}$$

where ω_s is the frequency of the input current source. This time interval ends when $V_x = V_{\rm dc}$, at which point the diode D_2 turns on. This occurs at time $u = \omega_s t$ given in radians by the following equation:

$$\cos(u) = 1 - \frac{\omega_s C_D V_{\rm dc}}{I_{\rm in}} = 1 - \frac{V_{\rm dc}}{X_C I_{\rm in}} \tag{8}$$

where X_C is the reactance of C_D at ω_s. When the polarity of the input current transitions from positive to negative, both diodes are off again and the current source discharges the capacitance

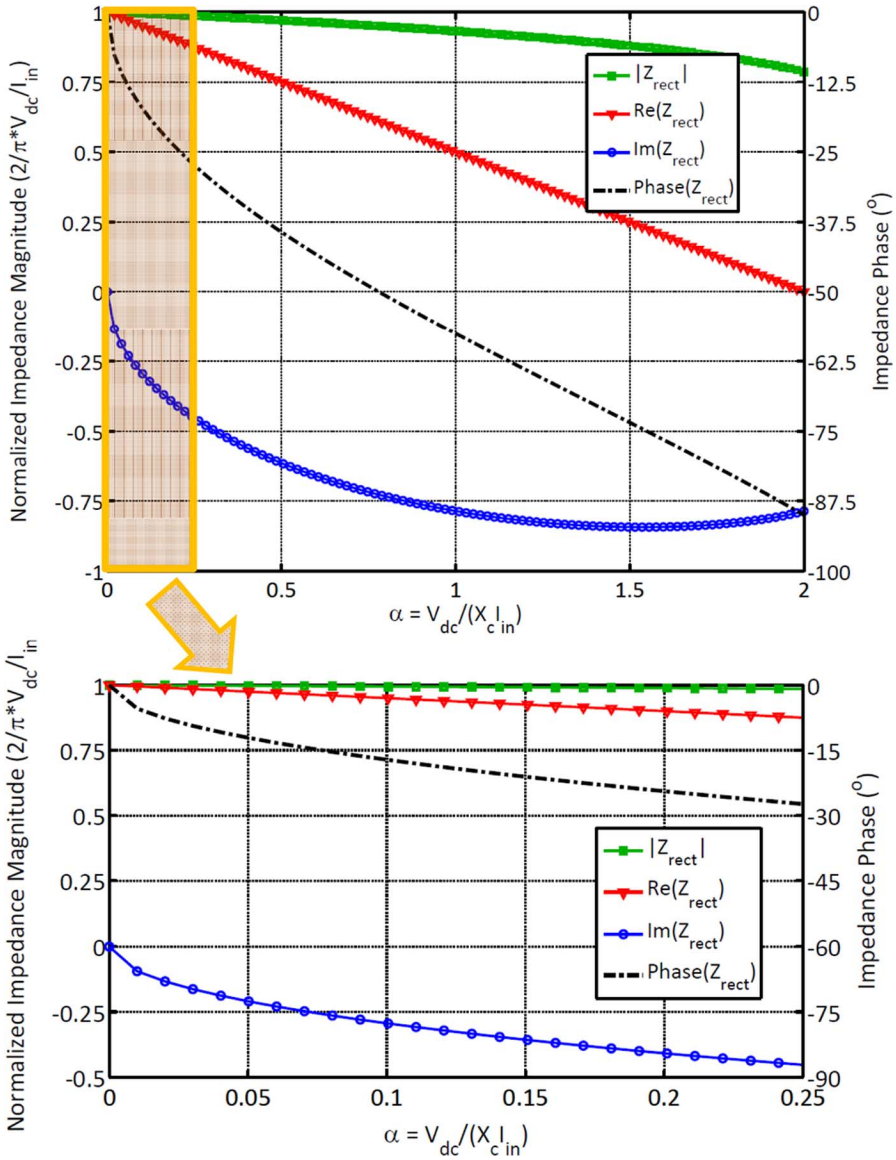

Fig. 8. Impedance of half-wave rectifier with parasitic capacitance versus parameter $\alpha = V_{\rm dc}/(X_c I_{\rm in})$. As α increases, the impedance looks increasingly capacitive.

C_D until $V_x = 0$ and diode D_1 turns on. During this time, V_x is given by

$$V_x(t) = V_{\rm dc} - \frac{I_{\rm in}}{\omega_s C_D}[1 - \cos(\omega_s t - \pi)]. \tag{9}$$

This time interval ends at time $\omega_s t = \pi + u$, where u is the same as in (8). Now that we have defined the input voltage V_x over the entire period, we can find the Fourier series coefficients of V_x at the fundamental frequency ω_s to be

$$a_{x1} = \frac{2}{\pi} V_{\rm dc}\left[-\frac{u}{2\alpha} + \left(\frac{1}{\alpha} - 1\right)\sin(u) - \frac{1}{4\alpha}\sin(2u)\right] \tag{10}$$

$$b_{x1} = \frac{2}{\pi} V_{\rm dc}\left[\frac{3}{4\alpha} + \left(1 - \frac{1}{\alpha}\right)\cos(u) + \frac{1}{4\alpha}\cos(2u)\right] \tag{11}$$

where $\alpha = V_{\rm dc}/(X_c I_{\rm in})$ and a_{x1} and b_{x1} represent the cosinusoidal and sinusoidal components (respectively) at the fundamental frequency (i.e., $V_{x1} = a_{x1} - jb_{x1}$). Using these equations together with Ohm's Law $Z = V/I$, we can calculate the rectifier impedance as follows:

$$|Z_{\rm rect}| = \frac{1}{I_{\rm in}}\sqrt{a_{x1}^2 + b_{x1}^2} \tag{12}$$

$$\angle(Z_{\rm rect}) = -\arctan\left(\frac{b_{x1}}{a_{x1}}\right) - \frac{\pi}{2}. \tag{13}$$

Fig. 8 shows the impedance of the half-wave rectifier with parasitic capacitance versus the parameter $\alpha = V_{\rm dc}/(X_c I_{\rm in})$ which we have defined (similar to "reactance factor" in low-frequency rectifiers [21]). If we substitute this parameter into (8), we can see that the diodes will no longer turn on when $\alpha > 2$, in which case the rectifier impedance will look purely capacitive with reactance X_C. This is evident in Fig. 8, which shows that as α increases from 0 to 2, the rectifier impedance transitions from purely resistive to purely capactive, as expected. Thus, a small value of α is desired to maintain a resistive rectifier impedance.

There are four parameters which determine the value of α: the operating frequency ω_s, the diode capacitance C_D, the input current $I_{\rm in}$, and the dc output voltage $V_{\rm dc}$. To minimize α, $I_{\rm in}$ should be maximized while ω_s, C_D, and $V_{\rm dc}$ should be minimized. However, these parameters are subject to several constraints. One constraint is the rectifier efficiency: because real diodes have a nonzero forward voltage drop, decreasing $V_{\rm dc}$ will lower the efficiency, and so maintaining a specified efficiency will set a lower bound on $V_{\rm dc}$. Another constraint is the maximum input power to the rectifier, which will determine the maximum value of $I_{\rm in}$ for a given $V_{\rm dc}$. Finally, once the values of $V_{\rm dc}$ and $I_{\rm in,max}$ are determined, the worst-case value of α will be determined by the operating frequency ω_s, the diode capacitance C_D, and the input power variation as given by the following equation:

$$\alpha_{\rm max} = \frac{\omega_s C_D V_{\rm dc}}{I_{\rm in,min}} = \omega_s C_D V_{\rm dc} \frac{c_{\rm power}}{I_{\rm in,max}} \tag{14}$$

where $c_{\rm power}$ is the ratio of the largest to smallest input power levels going into the rectifier. Thus, it is important to keep both the diode parasitic capacitance C_D and the operating frequency ω_s as small as possible. Unfortunately, this becomes difficult if high-frequency operation is required. One may conclude that the ratio $I_{f,\rm av}/C_T$ (rated current to device capacitance) is an important figure of merit for a diode in this application. A further figure of merit (having units of frequency) is $I_{f,\rm av}/(V_{D,\rm ON}C_T)$, where $V_{D,\rm ON}$ is the forward voltage drop of the diode.

One way to overcome this problem in high-frequency applications is to use a resonant rectifier topology [17], [19], [22], [23], which reduces the effect of the parasitic capacitance by removing the diode D_1 in Fig. 7(a) and replacing it with an inductor to tune out the parasitic capacitance (as well as provide a path for dc current). In this case, the bandwidth of the rectifier will be limited by the network Q of the RLC tank formed by inductor, diode capacitance, and equivalent rectifier resistance.

D. OPERA Efficiency

The total efficiency of the OPERA system is given by

$$\eta_{\rm tot} = \frac{P_{\rm out}}{P_{\rm dc} - P_{\rm rec}} \tag{15}$$

where $P_{\rm out}$ is the power delivered to the antenna load, $P_{\rm dc}$ is the dc power delivered to the PAs, and $P_{\rm rec}$ is the power sent back to the power supply from the RF-dc converter placed at the combiner's isolation port. The total power available from the PAs is

$$P_{\rm avail} = \eta_{\rm PA} P_{\rm dc} = P_{\rm out} + P_{\rm iso} \tag{16}$$

where $\eta_{\rm PA}$ is the PA efficiency and $P_{\rm iso}$ is the power delivered to the isolation port. Using (16), we can write $P_{\rm rec}$ as

$$P_{\rm rec} = \eta_{\rm rec} P_{\rm iso} = \eta_{\rm rec}(P_{\rm avail} - P_{\rm out}) \tag{17}$$

$$= \eta_{\rm rec}(\eta_{\rm PA} P_{\rm dc} - P_{\rm out}) \tag{18}$$

where $\eta_{\rm rec}$ is the energy recovery efficiency. Substituting (18) into (15), we can write the efficiency of the OPERA system as

$$\eta_{\rm tot} = \frac{P_{\rm out}}{P_{\rm dc} - \eta_{\rm rec}(\eta_{\rm PA} P_{\rm dc} - P_{\rm out})} \tag{19}$$

$$= \frac{p}{\frac{1}{\eta_{\rm PA}} - \eta_{\rm rec}(1-p)} \tag{20}$$

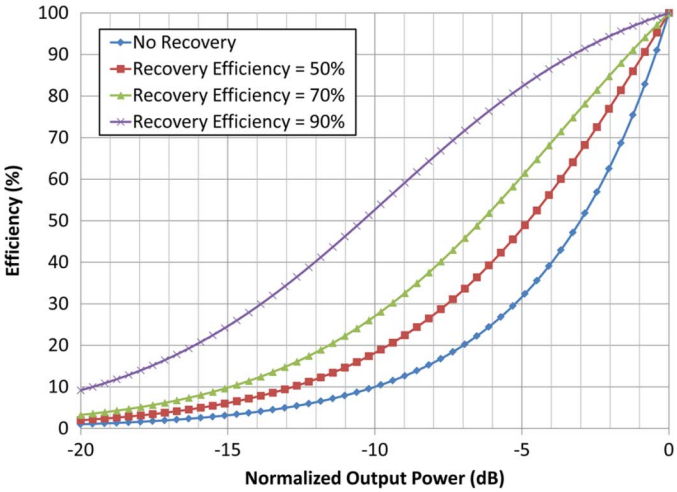

Fig. 9. Theoretical OPERA efficiency as a function of normalized output power, showing the effect of the energy recovery network efficiency.

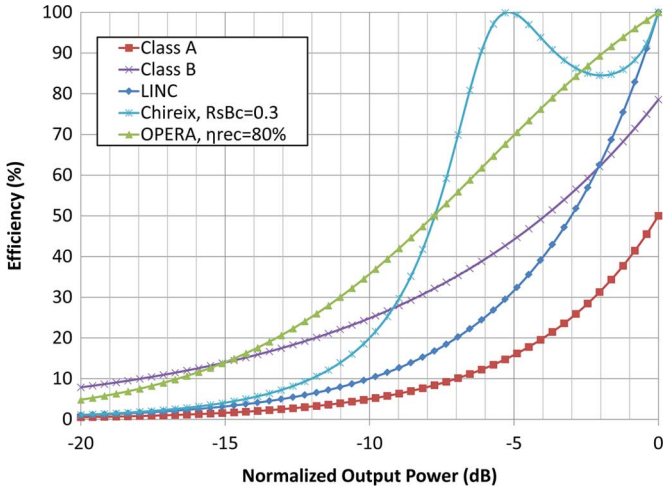

Fig. 10. Comparison of theoretical OPERA efficiency to that of other PA architectures. Note that the Chireix efficiency curve does not reflect the efficiency degradation that will occur due to the widely varying impedance presented to the outphased PAs as the output power varies.

where $p = P_{\rm out}/P_{\rm avail}$ is the normalized output power. To account for any insertion loss in the power combiner, it is sufficient to replace $\eta_{\rm PA}$ with $\eta_{\rm PA}\eta_{\rm comb}$, where $\eta_{\rm comb}$ is the efficiency of the power combiner.

Fig. 9 shows the predicted system efficiency in a LINC system with and without energy recovery. For illustrative purposes, the power amplifiers in the system are assumed to be 100% efficient, with no insertion loss in the combiner. As can be seen, the overall system efficiency is significantly enhanced by recycling the "wasted" power delivered to the isolation port of the combiner, and is strongly influenced by the efficiency of the energy recovery network, as one might expect. The amount of improvement will depend on the PAPR of the signal to be amplified.

The efficiency of the power recycling network will depend heavily on the power supply voltage, as well as on the series resistance of the diodes and their intrinsic cutoff frequency and built-in voltage [15] and the quality factors of the other passive components used in the RCN and impedance transformation network. Given the importance of the energy recovery efficiency

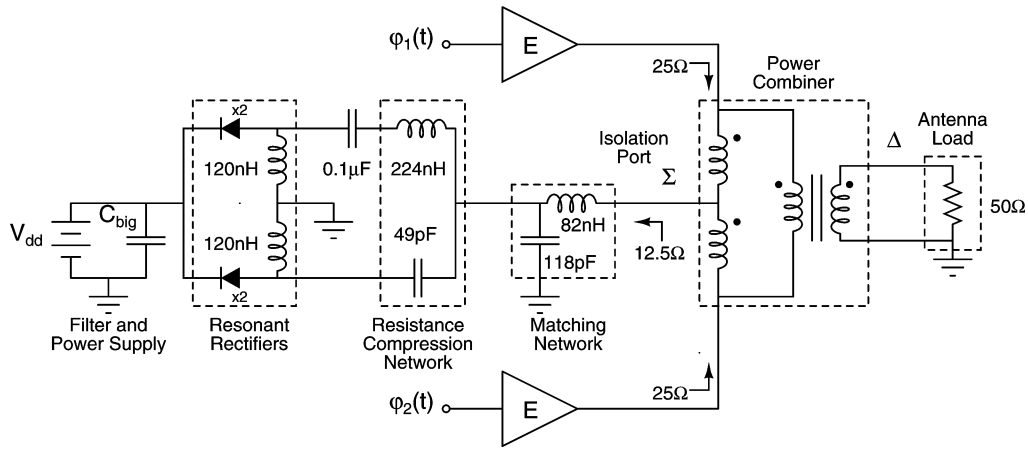

Fig. 11. Prototype OPERA system with resistance-compressed rectifier for energy recovery. Each rectifier branch is implemented with a pair of paralleled SS16 Schottky diodes. The impedance at each port of the power combiner that is required for matching and isolation is also indicated.

on the overall system efficiency, the fact that the resistance-compressed rectifier obviates the need for an additional isolator between the power recycling network and the combiner's isolation port is a key advantage of the OPERA system presented in this paper, because the loss introduced by the isolator is removed.

Fig. 10 compares the theoretical efficiency of the OPERA system with 80% recovery efficiency to that of other PA architectures. The OPERA efficiency is shown to be significantly higher than either class-A or class-B PAs. This can be attributed to the higher efficiency of the switched-mode PAs used in the LINC system, as well as enhanced efficiency due to the energy recovery network. It can also be seen that the OPERA system compares favorably to the Chireix outphasing PA (whose efficiency curve we have calculated from [12] for a given reactive compensation) when the entire power range is considered. This is due to the fact that the Chireix combiner can only be tuned for maximum efficiency around a single output power. It should also be noted that the Chireix combiner is nonisolating, making it generally incompatible with class-E PAs which have a high sensitivity to load variation [24]. Thus, the Chireix system must employ other PAs such as class D, class F,[1], or saturated class B which have generally lower efficiency. Furthermore, since the Chireix combiner presents a much wider impedance variation to the outphased PAs than the combiner in the OPERA system, both the linearity and PA efficiency will degrade significantly more. For these reasons, the efficiency of the Chireix system is even lower than suggested in Fig. 10.

III. OPERA Prototype

To demonstrate the feasibility of the OPERA system, a prototype was designed and implemented with discrete components at an operating frequency of 48 MHz. Fig. 11 shows a circuit schematic of the prototype OPERA system.

Fig. 12 shows the circuit schematic of the power amplifiers used in the OPERA prototype. Each PA is class-E, using an off-the-shelf RF power MOSFET, the ST Microelectronics PD57060, and designed for a supply voltage of 12 V with 10-W output power. Thus the maximum output power of the prototype outphasing PA is 20 W. Four parallel Fairchild NC7ZW04 CMOS inverters provide the gate drive. All inductors used in the prototype are air core spring inductors from Coilcraft.

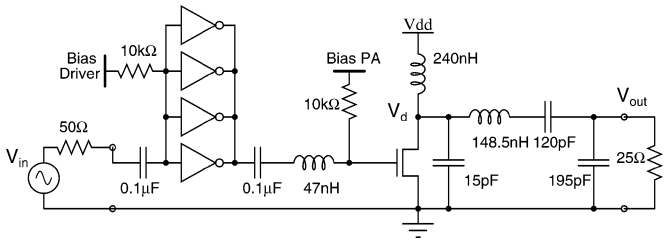

Fig. 12. Circuit schematic of the class-E power amplifier used in the OPERA prototype.

The power combiner used in the OPERA prototype consists of two 1 : 1 transformers, each implemented with 18AWG 5-turn bifilar windings on a Ferronics Cobalt-Nickel ferrite toroid core ("K" material with 0.9 inches outer diameter). The antenna load is connected to the difference port, while the power recycling network is connected to the summing port, which is the isolation port in this configuration. Fig. 11 shows the impedance at each port that is required for matching and isolation between the two outphased PAs. Fixing the antenna load at 50 Ω, the required impedances at the other ports can be found through even/odd (common/difference) mode analysis [25]. The prototype was also designed with the capability to switch the isolation port load between a fixed resistance and the power recycling network, in order to compare the standard LINC system shown in Fig. 1 with the OPERA system.

The rectifiers in the power recycling network in Fig. 11 are implemented with the resonant rectifier topology used in [17] and [19], in which a resonant inductor resonates with the diode capacitance so that the input looks resistive at the fundamental frequency. The resonant inductor also provides a path for dc current. Resonant rectifiers have several advantages over classical hard-switched (square-wave) rectifiers, including lower component count, lower parasitics, and higher efficiency [23]. The rectifiers use On-Semiconductor SS16 1A, 60-V Schottky diodes (two in parallel for each of the two rectifiers).

[1]Class-F PAs have a theoretical efficiency of 100%, but only if all odd harmonics are tuned in the output resonant filter [8] which is difficult to achieve in practical implementations. For example, with only the third harmonic tuned, the theoretical efficiency reduces to 88%.

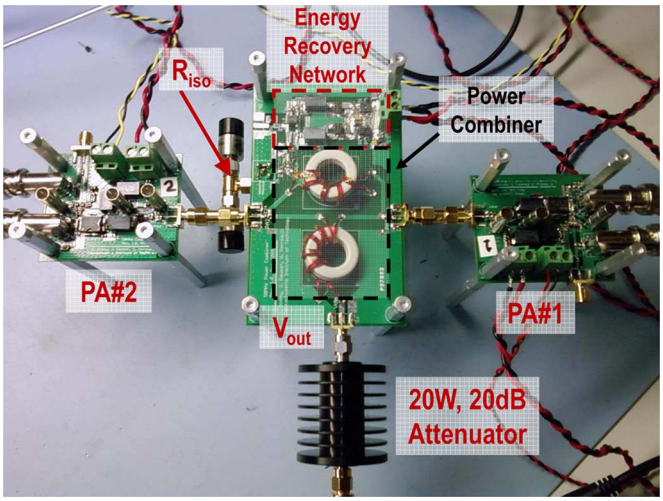

Fig. 13. Photograph of the prototype OPERA system.

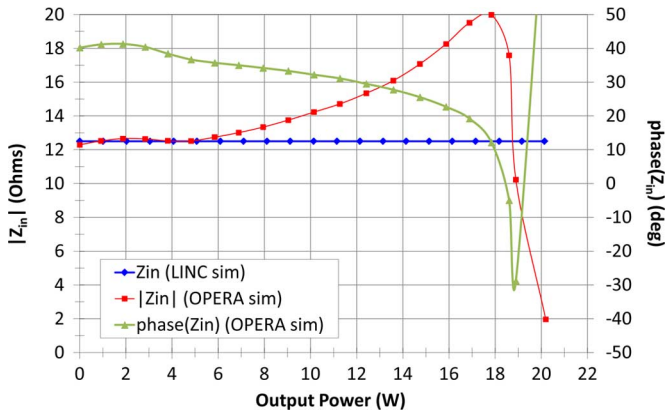

Fig. 14. Simulated isolation port impedance versus output power in the OPERA prototype. The desired isolation port impedance is also shown for reference.

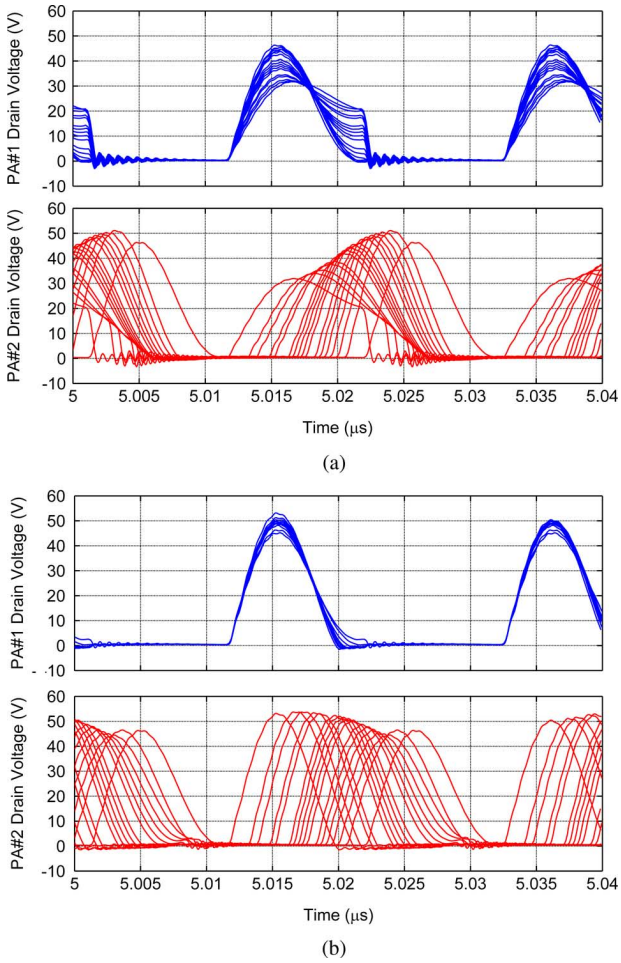

Fig. 15. Simulated PA drain voltages in the OPERA prototype with and without the resistance compression network, for various outphasing angles and output powers. (a) Energy recovery without RCN. (b) Energy recovery with RCN.

The conjugate reactances which comprise the RCN are implemented with a single capacitor and inductor. Alternatively, each reactance can be implemented with a series combination of an inductor and an capacitor as in [17] to provide additional filtering of the voltage harmonics created by the rectifiers, but it was found that the preceding matching network was sufficient for this purpose. The resistance-compressed rectifier was designed to keep the rectifiers operational over an input power range of 2–20 W, a 10 : 1 ratio in power. This corresponds to an impedance variation of 1.74 : 1 at the combiner's isolation port, as described in Section II. Besides providing harmonic filtering, the matching network transforms the compressed rectifier impedance to the level required by the power combiner.

Fig. 13 shows a photograph of the prototype OPERA system.

IV. Measurement Results and Discussion

Fig. 14 shows the simulated isolation port impedance versus output power in the OPERA prototype, measured as the ratio of the voltage and current at the fundamental of the operating frequency. The plot shows that the RCN compresses the impedance at the isolation port to a range between 12.5 Ω and 20 Ω from 0–18 W output power. Since the maximum output power of the system is 20 W, an output power range of 0–18 W corresponds to roughly 2–20 W input power to the resistance-compressed rectifier, a 10 : 1 variation (this is only an approximation because the power available from the PAs varies as the load impedance varies). Thus the RCN compresses a 10 : 1 impedance variation into a 1.6 : 1 variation. This agrees well with the thoeretical prediction of 1.74 : 1 calculated in Section II. Note that at the highest output powers, the isolation port impedance drops considerably. This is because in this case very little power is delivered to the rectifier and the diodes can no longer turn "on." However, as stated previously, this should not degrade the overall system efficiency and linearity because at these power levels most of the power from the PAs is delivered to the antenna load, and so the isolation port impedance has little effect.

Fig. 15 shows simulated PA drain voltages (denoted by V_d in Fig. 12) in the OPERA prototype with and without the RCN, for various outphasing angles and output powers. The waveforms show that the RCN helps to maintain zero-voltage switching (ZVS) in the class-E amplifiers, an important characteristic for achieving high efficiency. This demonstrates that the appropriate load impedance at the PA outputs is being maintained over the entire range of outphasing angles. It should be noted that the experimental system was essentially unuseable without

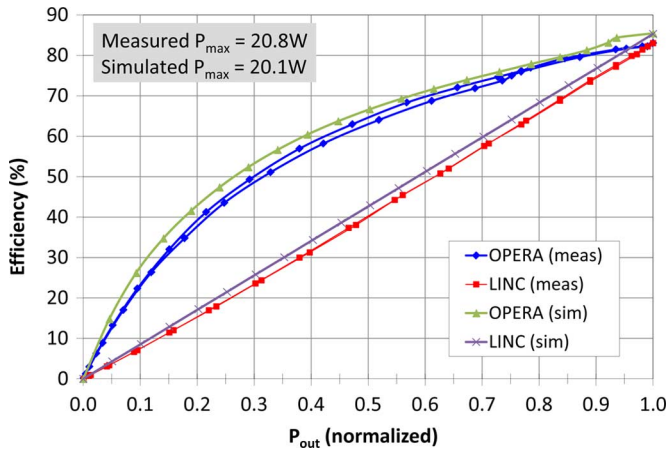

Fig. 16. System efficiency versus output power for the OPERA prototype.

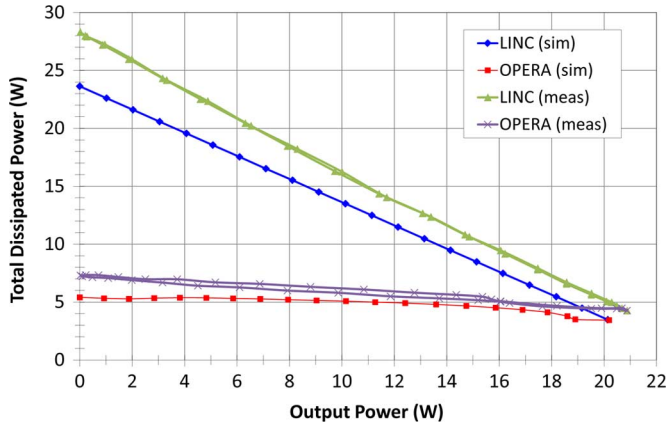

Fig. 17. Total dissipated power versus output power in the OPERA prototype with and without energy recovery.

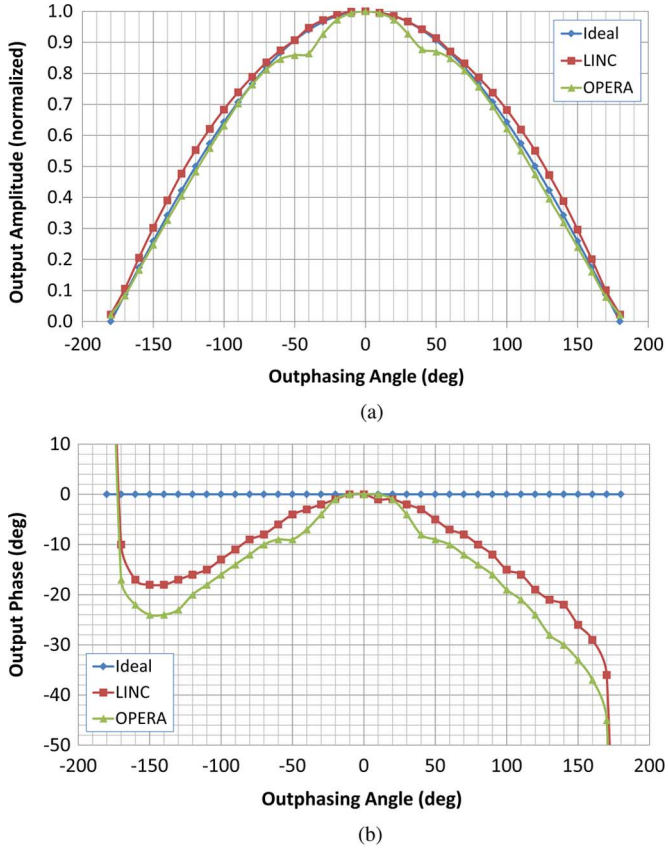

Fig. 18. Measured output amplitude and phase linearity for the OPERA prototype with and without energy recovery. (a) Output amplitude. (b) Output phase.

inclusion of the resistance compression network, owing to misoperation of the (load-sensitive) class-E amplifiers.

Fig. 16 shows both the simulated and measured system efficiency of the OPERA prototype versus output power, obtained by sweeping the outphasing angle from $-180°$ to $+180°$. For the purpose of comparison, the prototype was tested both with the isolation port connected to a fixed resistance (the standard LINC system) and to the power recycling network (the OPERA system). We can see that the simulated and measured efficiencies are in close agreement, and that the system efficiency is significantly enhanced when the power recycling network is used. The double curves in the case of the measured values are due to the mismatch between the two PAs in the prototype, resulting in different results for positive and negative outphasing angles. The prototype OPERA system achieves a peak power of 20.8 W, with a corresponding peak power-added efficiency of 82.9%. The efficiency of the energy recovery network varies from 78–89% for output powers up to 95% of the maximum. For output powers higher than this, the power going into the rectifiers is too low to turn the the diodes "on," resulting in a significant drop in the recovery efficiency.

Fig. 17 shows both the simulated and measured dissipated power versus output power in the LINC prototype with and without energy recovery. Again, we can see that the simulated and measured efficiencies are in close agreement, with the measured dissipated power somewhat higher due to the lower measured efficiency. The peak dissipated power of the OPERA prototype is reduced from 28.3 W without energy recovery to 7.3 W with energy recovery. This represents an energy savings of up to 4× when the OPERA system is used. As stated previously, the actual amount of energy savings will depend on the PAPR of the signal to be amplified. The energy savings has the additional benefit of significantly reducing the requirements of the heatsink used for any given application.

Fig. 18 shows the measured amplitude and phase of the output voltage at the fundamental of the RF output frequency versus the outphasing angle. The phase measurements are normalized to the output phase at maximum output power. The distortion present in both the LINC and OPERA cases is most likely due to the PA mismatch in the prototype. In another experiment, we measured the output power mismatch between the two PAs to be about 6%. Additionally, when energy recovery is used, we can see a significant distortion in the output for amplitudes between 85–95% of the maximum. As stated before, this is due to the fact that at higher output powers, very little power is delivered to the rectifiers and the diodes can no longer turn "on," and so the rectifier impedance can no longer be effectively compressed, resulting in distortion. This can also be understood by examining Fig. 14, which shows that in this operating region, the isolation port impedance deviates the most from the nominal value. It should be noted that for amplitudes greater than about 95% of the maximum, the distortion is reduced significantly. This is because in this case, almost all the power from

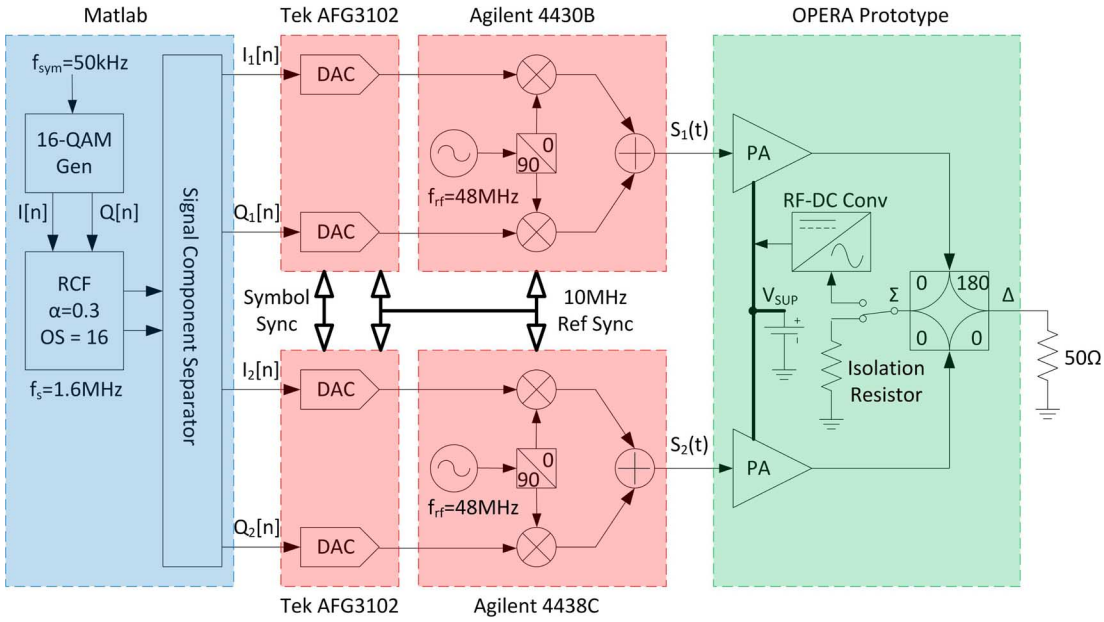

Fig. 19. Outphasing system testbench for 50-kHz 16-QAM transmission at a carrier frequency of 48 MHz.

the PAs is delivered to the antenna load, and so the isolation port becomes a virtual open circuit and its impedance has no effect. The static distortion exhibited by the OPERA prototype both with and without energy recovery can be significantly reduced with standard digital predistortion (PD) techniques [26]. In this work, a simple lookup table constructed from the data in Fig. 18 was sufficient to correct for this distortion.

To demonstrate the linearity of the OPERA system, we tested the prototype with a 50-kHz 16-QAM signal filtered with a raised cosine filter of rolloff 0.3, resulting in a signal PAPR of 6.5 dB. A block diagram of the testbench is shown in Fig. 19. The in-phase/quadrature (IQ) input sequences, including the signal separation functions, are created in MATLAB and uploaded into the internal memories of two Tektronix AFG3102 arbitrary function generators (AFGs). The signal separation incorporates the optimal outphase assignment scheme described in [27] which drastically reduces the amplitude variation of the two outphased signals $S_1(t)$ and $S_2(t)$. Each AFG feeds its baseband IQ outputs to the IQ inputs of an Agilent 4430 series vector signal generator (VSG) configured as an IQ modulator, which upconverts the baseband data to an RF carrier frequency of 48 MHz. The two RF signals are then fed to the two PAs in the OPERA prototype. The output of the OPERA prototype is fed into an HP 89400 vector signal analyzer (VSA) for spectrum and error vector magnitude (EVM) analysis.

Fig. 20 shows the measured output spectrum for the 50-kHz 16-QAM transmission from the OPERA prototype with and without energy recovery, both before and after predistortion. From the spectrum, we can see that there is very little degradation in the transmitted spectrum with the OPERA system as compared to the standard LINC system, both before and after the predistortion is applied. Fig. 21 shows the measured demodulated 16-QAM constellation of the OPERA prototype with and without energy recovery, both before and after predistortion. Again, we can see that before predistortion is applied, the degradation in EVM when energy recovery is used is small, only

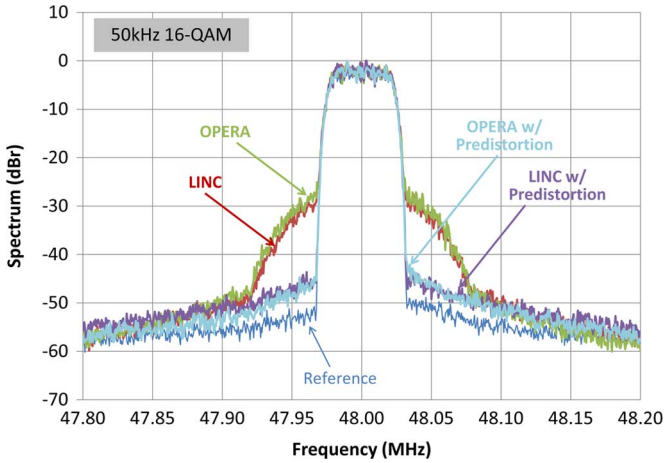

Fig. 20. Measured output spectrum for 50-kHz 16-QAM transmission with 6.5 PAPR, with and without energy recovery, and before and after predistortion. The reference spectrum is the result using only the combiner with a fixed isolation port resistance.

0.75%. After predistortion, the EVM both with and without energy recovery is reduced to less than 1%.

Table I summarizes the efficiency and linearity of the OPERA system in comparison with the standard LINC system. With energy recovery, the overall efficiency increases from 17.9% to 42.0%, and the dc power consumption is reduced from 27.3 to 11.7 W, representing an efficiency improvement and power savings of more than 2×.

One issue that has not been addressed to this point is the additional noise added to the power supply by the energy recovery network. This noise would show up in the measurement results as degraded EVM and a higher noise floor in the output spectrum. The spectrum and EVM measurements presented here suggest that the additional noise from the energy recovery network is negligible when compared with the standard

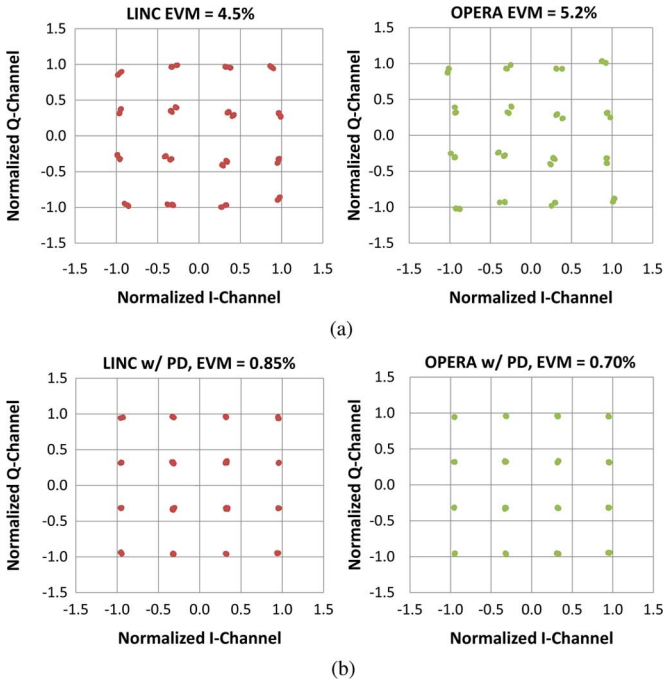

Fig. 21. EVM for the 50-kHz 16-QAM transmission for the OPERA prototype with and without energy recovery. (a) Before predistortion. (b) After predistortion.

TABLE I
16-QAM PERFORMANCE COMPARISON FOR LINC AND OPERA

Architecture	P_{dc}	P_{out}	η_{avg}	EVM
LINC	44.3dBm	37.5dBm	20.6%	4.5%
OPERA	40.6dBm	36.5dBm	39.6%	5.2%
LINC w/ PD	44.4dBm	36.9dBm	17.9%	0.85%
OPERA w/ PD	40.7dBm	36.9dBm	42.0%	0.70%

LINC system. In general, this noise should not effect the overall performance if appropriate filtering (e.g., bypass capacitance or full EMI filtering) is applied.

Since these measurement results were obtained at 48 MHz, it is important to discuss the effectiveness of the OPERA system at higher operating frequencies (e.g., in the microwave range). The system efficiency will most likely degrade due to the generally lower PA efficiencies obtained in this frequency range as well as the higher insertion loss resulting from high-frequency parasitics. However, as long as the efficiency of the PA and energy recovery network remains high enough, the efficiency improvement should still be significant and can be predicted by (20). As PA peak efficiencies of up to 80% have been reported at an RF frequency of 2 GHz [9], [28], and rectifier efficiencies as high as 75% have been reported at frequencies up to 10 GHz [29], [30], it is likely that system efficiencies similar to those presented in this paper can be obtained in the microwave frequency range.

V. CONCLUSION

We have demonstrated a new outphasing energy recovery amplifier which greatly increases system efficiency while maintaining high linearity. Higher efficiency is obtained by replacing the isolation resistor in the conventional matched combiner with a rectifier, which recovers the untransmitted power that is usually wasted back to the power supply. Linearity is maintained through the use of a resistance-compression network, which reduces the impedance variation of the rectifier in order to provide isolation and matching between the two outphased PAs. A prototype system was designed and built at a carrier frequency of 48 MHz, delivering 20.8-W peak power with 82.9% PAE. The prototype is tested with a 50-kHz 16-QAM signal with a PAPR of 6.5 dB and improves the overall efficiency from 17.9% to 42.0% over the standard LINC system.

ACKNOWLEDGMENT

The authors would like to thank SungWon Chung, Tony Sagneri, and Yehui Han at MIT for helpful discussions.

REFERENCES

[1] H. Chireix, "High-power outphasing modulation," *Proc. IRE*, vol. 23, pp. 1370–1392, Nov. 1935.
[2] D. C. Cox, "Linear amplification with nonlinear components," *IEEE Trans. Commun.*, vol. COM-23, pp. 1942–1945, Dec. 1974.
[3] N. Sokal and A. Sokal, "Class E—A new class of high-efficiency tuned sinle-ended switching power amplifiers," *IEEE J. Solid-State Circuits*, vol. SC-10, no. 3, pp. 168–176, Jun. 1975.
[4] N. Sokal, "Class-E RF power amplifiers," *QEX*, pp. 9–20, Jan./Feb. 2001.
[5] V. Tyler, "A new high-efficiency high-power amplifier," *Marconi Rev.*, vol. 21, no. 130, pp. 96–109, 3rd quarter 1958.
[6] R. H. Raab, "Class-F power amplifiers with maximally flat waveforms," *IEEE Trans. Microw. Theory Tech.*, vol. 45, no. 11, pp. 2007–2012, Nov. 1997.
[7] K. Honjo, "A simple circuit synthesis method for microwave class-F ultra-high-efficiency amplifiers with reactance-compensation circuits," *Solid-State Electron.*, vol. 44, no. 8, pp. 1477–1482, Aug. 2000.
[8] S. Kee, I. Aoki, A. Hajimiri, and D. Rutledge, "The class E/F family of ZVS switching amplifiers," *IEEE Trans. Microw. Theory Tech.*, vol. 51, no. 6, pp. 1677–1690, Jun. 2003.
[9] F. Lepine, A. Adahl, and H. Zirath, "L-band LDMOS power amplifiers based on an inverse class-F architecture," *IEEE Trans. Microw. Theory Tech.*, vol. 53, no. 6, pp. 2007–2012, Jun. 2005.
[10] J. W. Phinney, D. J. Perreault, and J. H. Lang, "Radio-frequency inverters with transmission-line input networks," in *Proc. 37th IEEE Power Electron. Spec. Conf.*, Jun. 2006, pp. 3211–3219.
[11] J. M. Rivas, Y. Han, O. Leitermann, A. Sagneri, and D. J. Perreault, "A high-frequency resonant inverter topology with low-voltage stress," *IEEE Trans. Power Electron.*, vol. 23, no. 4, pp. 1759–1771, Jul. 2008.
[12] I. Hakala, D. K. Choi, L. Gharavi, N. Kajakine, J. Koskela, and R. Kaunisto, "A 2.14-GHz Chireix outphasing transmitter," *IEEE Trans. Microw. Theory Tech.*, vol. 53, no. 6, pp. 2129–2138, Jun. 2005.
[13] F. H. Raab, "Efficiency of outphasing RF power-amplifier systems," *IEEE Trans. Commun.*, vol. 33, no. 9, pp. 1094–1099, Sep. 1994.
[14] S. Moloudi, K. Takinami, M. Youssef, M. Mikhemar, and A. Abidi, "An outphasing power amplifier for a software-defined radio transmitter," in *Proc. Int. Solid-State Circuits Conf. Tech. Dig.*, Feb. 2008, pp. 568–636.
[15] R. Langridge, T. Thornton, P. M. Asbeck, and L. E. Larson, "A power re-use technique for improved efficiency of outphasing microwave power amplifiers," *IEEE Trans. Microw. Theory Tech.*, vol. 47, no. 8, pp. 1467–1470, Aug. 1999.
[16] X. Zhang, L. E. Larson, P. M. Asbeck, and R. A. Langridge, "Analysis of power recycling techniques for RF and microwave outphasing power amplifiers," *IEEE Trans. Circuits Syst. II*, vol. 49, no. 5, pp. 312–320, May 2002.
[17] Y. Han, O. Leitermann, D. A. Jackson, J. M. Rivas, and D. J. Perreault, "Resistance compression networks for radio-frequency power conversion," *IEEE Trans. Power Electron.*, vol. 22, no. 1, pp. 41–53, Jan. 2007.
[18] R. Steigerwald, "A comparison of half-bridge resonant converter topologies," *IEEE Trans. Power Electron.*, vol. PE-3, no. 2, pp. 174–182, Apr. 1988.
[19] R. M. Rivas, D. Jackson, O. Leitermann, A. D. Sagneri, Y. Han, and D. J. Perreault, "Design considerations for very high frequency dc-dc converters," in *Proc. 37th IEEE Power Electron. Spec. Conf.*, Jun. 2006, pp. 2287–2297.

[20] D. Hamill, "Class DE inverters and rectifiers for dc-dc conversion," in *Proc. 27th IEEE Power Electron. Spec. Conf.*, Jun. 1996, pp. 23–27.
[21] J. G. Kassakian, M. F. Schlecht, and G. C. Verghese, *Principles of Power Electronics*. Reading, MA: Addison-Wesley, 1992, ch. 3.
[22] R. Gutmann and J. Borrego, "Power combining in an array of microwave power rectifiers," *IEEE Trans. Microw Theory Tech.*, vol. MTT-27, no. 12, pp. 958–968, Dec. 1979.
[23] W. A. Nitz, W. C. Bowman, F. T. Dickens, F. M. Magalhaes, W. Strauss, W. B. Suiter, and N. G. Ziesse, "A new family of resonant rectifier circuits for high frequency dc-dc converter applications," in *Proc. Applied Power Electron. Conf.*, Feb. 1988, pp. 12–22.
[24] J. Yao and S. I. Long, "Power amplifier selection for LINC applications," *IEEE Trans. Circuits Syst. II*, vol. 53, no. 8, pp. 763–767, Aug. 2006.
[25] T. H. Lee, *Planar Microwave Engineering*. Cambridge, U.K.: Cambridge Univ. Press, 2004, ch. 7.
[26] S. Chung, J. W. Holloway, and J. L. Dawson, "Energy-efficient digital predistortion with lookup table training using analog Cartesian feedback," *IEEE Trans. Microw. Theory Tech.*, vol. 56, no. 10, pp. 2248–2258, Oct. 2008.
[27] A. Pham, G. W. Wornell, and C. G. Sodini, "A digital amplitude-to-phase conversion for high-efficiency linear outphase power amplifiers," in *Proc. Int. Conf. Acoustics, Speech, Signal Process.*, May 2006, vol. 4, pp. IV–IV.
[28] D. Kimball, J. Jeong, C. Hsia, P. Draxler, S. Lanfranco, W. Nagy, K. Linthicum, and L. Larson, "High-efficiency envelope-tracking W-CDMA base-station amplifier using GaN HFETs," *IEEE Trans. Microw. Theory Tech.*, vol. 54, no. 11, pp. 3848–3856, Nov. 2006.
[29] Y.-J. Ren and K. Chang, "5.8-GHz circularly polarized dual-diode rectenna and rectenna array for microwave power transmission," *IEEE Trans. Microw. Theory Tech.*, vol. 54, no. 4, pp. 1495–1502, Apr. 2006.
[30] X. Yang, J. Xu, D. Xu, and C. Xu, "X-band circularly polarized rectennas for microwave power transmission applications," *J. Electron. (China)*, vol. 25, no. 3, pp. 389–393, May 2008.

Philip Godoy (S'05) was born in Warren, MI, in 1984. He received the B.S. degree in electrical engineering and computer science from the University of California, Berkeley, in 2006 and the S.M. degree in electrical engineering from the Massachusetts Institute of Technology (MIT), Cambridge, in 2008. He is currently pursuing the Ph.D. degree at MIT.

In 2006, he worked for Broadcom Corporation, San Jose, CA on data converters. His research interests include RF, analog, and digital circuits, particularly digitally assisted RF systems.

David J. Perreault (S'91–M'97–SM'06) received the B.S. degree from Boston University, Boston, MA, in 1989, and the S.M. and Ph.D. degrees from the Massachusetts Institute of Technology, Cambridge, in 1991 and 1997, respectively.

In 1997 he joined the MIT Laboratory for Electromagnetic and Electronic Systems as a Postdoctoral Associate, and became a Research Scientist in 1999. In 2001, he joined the MIT Department of Electrical Engineering and Computer Science, where he is presently an Associate Professor. His interests include design, manufacturing, and control techniques for power electronics, and in their use in a wide range of applications.

Joel L. Dawson (S'96–M'04) received the S.B. degree in electrical engineering from the Massachusetts Institute of Technology (MIT), Cambridge, in 1996, and the M.Eng. degree from MIT in electrical engineering and computer science in 1997. He went on to pursue further graduate studies at Stanford University, Stanford, CA, where he received the Ph.D. degree in electrical engineering for his work on power amplifier linearization techniques.

He is currently an Associate Professor in the Department of Electrical Engineering and Computer Science, MIT. Before joining the faculty at MIT in 2004, he spent one year at Aspendos Communications, a startup company that he cofounded. He continues to be active in the industry as both a technical and legal consultant.

Prof. Dawson received the NSF CAREER award in 2008.